RSC Advances

ROYAL SOCIETY OF CHEMISTRY

www.rsc.org/advances

Journal Name

ARTICLE

A new strategy to tailor the structure of sustainable 3D hierarchical porous N-self-doped carbons from renewable biomass for high-performance supercapacitors and CO_2 capture

Received 00th January 20xx,
Accepted 00th January 20xx

DOI: 10.1039/x0xx00000x

www.rsc.org/

Xing Tong,[a] Hao Zhuo,[a] Sha Wang, [a] Linxin Zhong,*[a] Yijie Hu,[a] Xinwen Peng,*[a] Weijia Zhou[b] and Runcang Sun[c]

Hierarchical porous N-doped carbons show great potential applications in energy storage and CO_2 capture. Renewable biomass chitosan that is abundant and simultaneously contains large amounts of N and C is an ideal alternative to fossil resources for sustainable and scale-up production of cost-effective N-self-doped carbons. In this work, we employed a new and effective strategy to obtain 3D hierarchical porous N-self-doped carbons from chitosan. The hierarchical porous structure of the N-self-doped carbons could be easily tailored to obtain nanorod interconnected and fiber-wall interconnected architectures without using any porogen, catalyst or activator. The nanorod interconnected porous carbon displayed a high specific surface area of 1408 m^2/g while the fiber-wall interconnected porous carbon exhibited an excellent specific capacitance of 261 F/g (0.5 A/g) due to the desirable hierarchical framework. In addition, these hierarchical porous carbons had a good CO_2 capture performance (3.07~3.44 mmol/g at 25 ℃). This unique method is supposed to be a new strategy to create novel 3D hierarchical porous carbons for promising applications in supercapacitors, lithium ion batteries, fuel cells and sorbents.

Introduction

Supercapacitor has attracted extensive attention for new generation energy storage systems because of their high power density, long cycling stability, and fast charge-discharge rate[1-4]. Porous carbons show various advantages such as high specific surface area, excellent conductivity, physicochemical structure stability, low density, and low cost, making them ideal alternatives for electrical double-layer supercapacitors[5,6]. Among various porous carbons, 3D hierarchical porous carbons with various pores ranging from nano-meter to micro-meter are particularly promising because they possess tunable porous structure and excellent conductivity[7]. The micro- and mesopores can provide large quantities of active sites for ion adsorption while the macropores guarantee the accessibility of these active sites to ions. Therefore, 3D hierarchical porous carbons allow the efficient diffusion and adsorption of electrolyte ions and electrons[1,8,9]. Various 3D hierarchical porous carbons such as graphene aerogels[10-12] and nanotube aerogels[13-15] inspire great interest and display excellent supercapacitor performances.

In recent years, heteroatom doping such as N, B, S, and P is found to effectively adjust the physicochemical structure and properties of carbon materials, and especially improve their adsorption performances, electrochemical activity, and catalytic behaviors[16-18]. Among these heteroatom-doped carbons, N-doped carbons attract particular attention. N-doped carbons present excellent oxidation stability, conductivity, adsorption, wettability, and electrocatalytic activity due to the small atom size, low electronegativity, and high charge density of doped N. Furthermore, the conjugation of lone-pair electrons of N and graphitic π-bonds in the carbons destruct carbon framework and create more active sites and defects[16,18,19]. Therefore, N-doped carbons with excellent supercapacitance behaviors attract extensive attention[20-22]. Traditional N-doped carbons are usually prepared by doping porous carbons with N-containing compounds such as ammonia[23], acrylonitrile[24], urea[25], and melamine[26], or directly carbonizing C and N-containing compounds such as ionic liquid[27], polypyrrole[28], and polyacrylonitrile[29], etc. However, these N-doped methods require large amounts of high-cost petroleum-based resources, and thus are not sustainable and cost-effective routs for large-scale production of N-doped carbons.

Renewable biomass is the most abundant, inexhausted, and low-cost as well as environmentally friendly resource on the earth. Biomass resources that simultaneously contain large amounts of N and C are ideal alternatives to fossil resources for sustainable and scale-up production of cost-effective N-doped carbons. The predominant advantage is that high N-containing carbons can be

[a] State Key Laboratory of Pulp and Paper Engineering, South China University of Technology, Guangzhou, P. R. China.
[b] School of environment and energy, South China University of Technology, Guangzhou, P. R. China.
[c] *Beijing Key Laboratory of Lignocellulosic Chemistry, Beijing Forestry University, Beijing,China*
** Author to whom correspondence should be addressed: L. X. Zhong, Email: lxzhong0611@scut.edu.cn; X. W. Peng, Email: fexwpeng@scut.edu.cn*
Electronic Supplementary Information (ESI) available: [Cycling charge-discharge performance of porous carbon]. See DOI: 10.1039/x0xx00000x

cost-effectively obtained by a simple one-step way without additions of high-cost and toxic C and N sources. Recently, such biomass-derived N-self-doped carbons have attracted great interest for supercapacitor applications, and various biomass resources such as microbe[30,31], protein[32-34], gelatin[35], and dopamine[36] have been used as C and N precursors. Although these N-self-doped carbons exhibited high capacity (higher than 200 F/g), their precursors are relatively high-cost and cannot be widely available in large scale.

Chitin and its derivative chitosan, originating from the cells of various crustaceans such as shrimp, crab, and insect, are the most abundant and low-cost resources on the earth. They are the most promising raw materials for cost-effectively manufacturing N-self-doped porous carbons for supercapacitors in large scale. Nguyen et al.[37] used chitin as a precursor and nano silica as a porogen to fabricate N-self-doped porous carbon with a high specific surface area (about 1000 m^2/g) and a relatively high specific capacitance of 154 F/g (0.46 A/g). N-self-doped porous carbon prepared from chitosan by using nano silica as a porogen and nickel nitrate as a catalyst showed a high specific capacitance of 222 F/g (0.5 A/g)[38]. In addition, by using nano silica as a porogen and $ZnCl_2$ as an activator could produce N-self-doped carbon with a high specific surface area of 1574 m^2/g and a specific capacitance of 202 F/g (20 mV/s) from chitosan[39]. Since raw materials chitin and chitosan are compact and have few pores, micropores and/or mesopores in these carbons were mainly created by porogen and/or activation. The monistic pores in these carbons disfavor the efficient diffusion of electrolyte ions and electrons. It was found that the increase in specific surface area could not always positively enhance the specific capacitance, because with increasing specific surface area, the micropore volume increased and the micropore size decreased below the size of hydrated electrolyte ions, which decreased the accessibility of pores[40]. Therefore, the hierarchical porous structure with multi-scale pores favors the diffusion and storage of ions[41]. However, to the best of our knowledge, the only report on the synthesis of hierarchical N-self-doped carbon from chitosan was by Hao et al[42]. In their work, hierarchical porous N-self-doped carbon aerogel with macro-, meso- and micropores was prepared from chitosan for high-performance supercapacitor using a freeze-drying and subsequent KOH activation process. Although the porous N-self-doped carbon had a very high specific surface area of 2435.2 m^2/g, the specific capacitance was only about 175 F/g at 0.5 A/g.

In this work, we employed an innovative and unique method (dissolving-gelling) to obtain novel 3D hierarchical porous N-self-doped carbons with desirable structure. In contrast to the previously reported method with only dissolving and directly freeze-drying in aqueous acetic acid, this dissolving-gelling process involved not only chitosan dissolving via a new method (NaOH/urea/H_2O at low temperature), but also a unique gelling step at room temperature. By introducing this gelling step, a nanofibril interconnected network was created due to the aggregation behavior of chitosan chains, and thus creating hierarchical porous chitosan aerogels and N-self-doped carbons. Due to the unique hierarchical porous structures, These N-self-doped carbons displayed either high specific area or high specific capacitance that is much higher than those of other chitosan-derived N-self-doped porous carbons reported previously. In addition, we also showed that these hierarchical porous carbons had a good CO_2 capture performance.

Materials and methods

Materials

The chitosan (deacetylation ≥ 85%, the viscosity is about 200 cps) was purchased from Aladdin, China. Other reagents were analytical grade and used without further purification.

Preparation of N-self-doped porous carbons

(a) Purification of chitosan. 2 g chitosan powder was dissolved in 100 g aqueous acetic acid (2%, v/v). After completely dissolution, the chitosan solution was neutralized by 2 wt% sodium hydroxide aqueous solution and washed with deionized water until a neutral pH was achieved. Finally, the purified chitosan was obtained after freeze-drying.

(b) Preparation of chitosan carbon aerogel by using water as a freezing medium. 1 g of the purified chitosan was added into 49 mL NaOH/urea/water solution (the mass ratio of NaOH: urea: H_2O was 8: 4: 88). After vigorously stirring at room temperature for half an hour, the mixture was placed in a refrigerator and frozen at -20 °C for 4 h. Afterwards, the frozen solution was stirred at 0 °C until a transparent solution was obtained. When the viscous solution soon congealed into hydrogel at room temperature, the hydrogel was then washed with deionized water to remove the residual alkali and urea completely. After being frozen in liquid nitrogen, the sample was freeze-dried in a lyophilizer (-58 °C, 0.22 mbar) for 48 h to obtain chitosan aerogel. The carbonization of the chitosan aerogel was performed in a tubular furnace. The chitosan aerogel was first heated to 200 °C at a heating rate of 5 °C min^{-1} under N_2 atmosphere and held for 2 h. Then the sample was pyrolyzed from 200 to 800 °C at a heating rate of 3 °C min^{-1} and held at 800 °C for another 2 h to obtain carbon aerogel (CS-W).

(c) Preparation of chitosan carbon aerogel by using tert-butyl alcohol as a freezing medium. Chitosan hydrogel was synthesized and purified using the same method above, and then was placed in tert-butanol to replace deionized water completely before being frozen at -20 °C for 1 h. The frozen sample was freeze-dried in a lyophilizer (-58 °C, 0.22 mbar) for 48 h. The carbonization was carried out in the same way as mentioned above to obtain CS-OH.

(d) Preparation of chitosan carbon aerogel (CS-AC) by directly freeze-drying aqueous chitosan/acetic acid. 1 g of chitosan powder was first dissolved in 49 mL acetic acid aqueous solution (2%, v/v). Then the solution was immersed into liquid nitrogen and freeze-dried in a lyophilizer (-58 °C, 0.22 mbar) for 48 h. The carbonization was carried out in the same way as mentioned above.

Characterizations

X-ray diffraction (XRD) patterns were monitored by a Bruker D8 diffractometer using Cuα radiation (λ = 0.15418 nm) as an X-ray source. The specific surface area (BET) and CO_2 uptake (25 °C) were evaluated by using a physisorption analyzer (Micromeritics ASAP 2020). Prior to each adsorption experiment, sample was degassed at 200 °C for several hours to ensure that the residual pressure was

below 1×10^{-3} mbar. The morphology was observed from transmission electron microscopy (TEM, JEM-2100F) and scanning electron microscope (SEM, Merlin, Zeiss). Raman spectra were recorded on a Raman spectrometer (LabRAM ARAMIS, H.J.Y) operating with 532 nm laser. The element contents were measured by an elemental analyzer (VarioEL III, Elementar). X-ray photoelectron spectra (XPS) were recorded on Thermo Scientific ESCALAB 250Xi spectrometer with an exciting source of Al·Kα (1286.6 eV).

Electrochemical measurements

The monolithic carbon aerogels were cut into small slices with a dimension of about 1 mm × 10 mm × 10 mm, and pressed onto titanium meshes as working electrodes. Cyclic voltammetry, galvanostatic charge/discharge, and electrochemical impedance spectroscopy were carried out on an electrochemical workstation (CHI660E Chenhua Instruments Co., Ltd., Shanghai, China) in 1.0 M H_2SO_4 aqueous solution using three-electrode system at room temperature. An Ag/AgCl electrode and a platinum wire were used as the reference and counter electrodes, respectively. The frequency range for the impedance spectra was from 0.01 Hz to 100 kHz. The specific capacitance was calculated from CV curve according to the equation (1):

$C=(\int I dV)/(vm\Delta V)$ (1)

Where I is the current (A), v is the scanbing rate (V/s), ΔV is the applied potential window (V), and m (g) is the mass of the active material in working electrode.

The specific capacitance from galvanostatic charge/discharge curve was calculated according to the equation (2):

$C=(I\Delta t)/(m\Delta V)$ (2)

Where I is current loaded (A), Δt is the discharge time (s), m (g) is the mass of the active material in working electrode, and ΔV is the range of potential (V).

Results and discussion

Physicochemical structures of hierarchical porous carbons

The microstructures of the as-prepared hierarchical porous carbons are shown in Figure 1. Figure 1a and 1b show that CS-AC possesses cellular honeycomb-like structure with uniform 3D interconnected unidirectional channels (ca. 10 um). Large amounts of sheets align along the freezing direction and stack together to form interconnected channel. CS-AC was fabricated by dissolving chitosan, directly freeze-drying in acetic acid solution, and then carbonizing without gelling step. In this case, no interconnected nanofibrils were formed since the interactions (mainly hydrogen bonds) among chitosan chains could not form in aqueous acetic acid. Furthermore, the solidification of aqueous acetic acid in the freezing step before freeze-drying required a relatively long time period, because the freezing point of aqueous acetic acid is low, resulting in large crystals that grew along the freezing direction (Scheme 1). The formation and growth of these crystals extruded chitosan chains aside into sheets, forming a structure that crystals were encapsulated by chitosan shells. The removal of these crystals led to a unidirectedly lamellar structure as well as large and thick sheets. Therefore, CS-AC is mainly composed of unidirectional macro channels. Similar result was also reported by Hao et al[42].

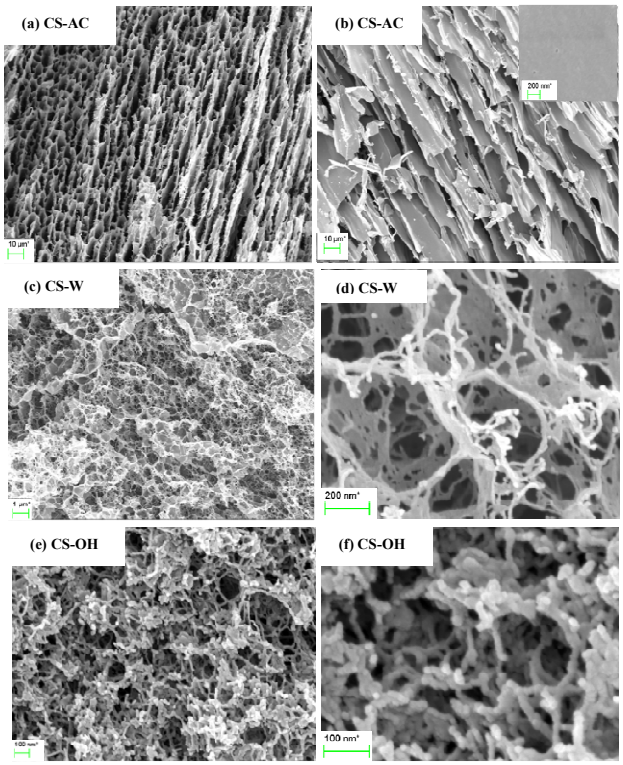

Figure 1. SEM images of the hierarchical porous networks of CS-AC (a and b), CS-W (c and d), and CS-OH (e and f).

CS-W obtained via unique dissolving-gelling method, however, shows a completely different hierarchical porous structure from CS-AC, as shown in Figure 1c and 1d. A great number of well-developed mesopores and open macropores are observed on the pyrolytic carbon. In fact, CS-W consists of nano carbon fiber network cross-linked with carbon lamina. The most unique feature of this dissolving-gelling method is that chitosan can not only be dissolved in NaOH/urea/H_2O solution at low temperature (-20 °C) but also easily gel at room temperature because chitosan chains are very unstable at room temperature and tend to aggregate into nanofibrils due to the strong interaction between chitosan chains (hydrogen bonds). A faster crystallization speed of H_2O than that of aqueous acetic acid in the frozen step before freeze-drying resulted in much smaller ice crystal particles. Although the extrusion of nanofibrils also occurred during the formation and growth of ice crystals, this effect was less significant because the ice crystal particles were much smaller (as a result of lower freezing point) as compared with the acetic acid/H_2O crystals. Therefore, the removal of the ice crystals by freeze-drying produced a hierarchical porous aerogel with fiber-wall interconnected architecture. The N-self-doped carbon inherited such a hierarchical porous architecture of chitosan aerogel, and possessed much smaller pores from nano-meter to micro-meter after carbonzation. This porous feature could not be achieved when using aqueous acetic acid as a dissolving solvent and freezing medium because chitosan chains could not

aggregate in aqueous acetic acid (protonated amino groups disfavored the aggregation of chitosan chains). Such a long-range continuity of the pore network is expected to permit the electrolytes to transfer fast throughout the material and decrease the diffusion distance of ions, and thus enhance the dynamic performance and electrochemical properties of the material.

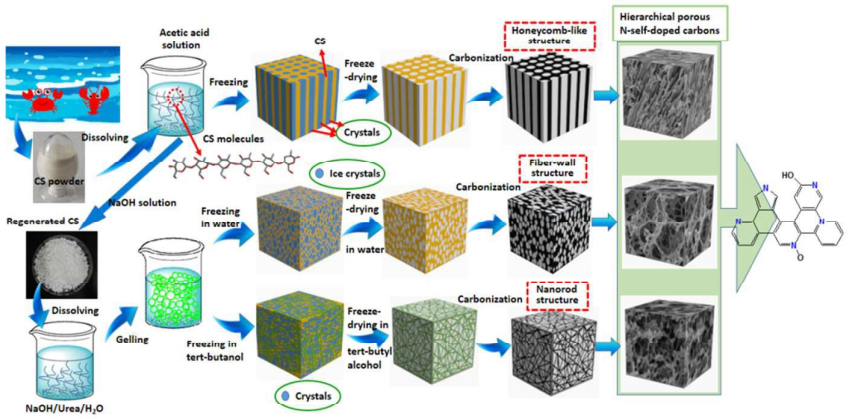

Scheme 1. Preparing and tailoring the structure of 3D hierarchical porous N-self-doped carbons from chitosan.

Interestingly, by replacing H_2O with tert-butanol as a freezing medium, a distinct porous structure mainly composed of interconnected nanorods (10-30 nm) could be created, as shown in Figure 1e and 1f. This unique structure can be attributed to the high freezing point of tert-butanol (above 25 ℃). When the chitosan gel saturated with tert-butanol was frozen, high freezing point of tert-butanol made it very quickly solidify with much smaller particles as compared with ice crystals resulting from H_2O. These smaller particles led to less significant extrusion of the interconnected nanofibrils, and thus the chitosan aerogel could maintain the nanofibrils interconnected structure. Volume shrinkage due to the losses of O, H, N, and C during carbonization at high temperature resulted in a nanorod interconnected structure. This type of porous carbon has never been reported before, and is expected to possess high surface area. Overall, our results indicate that gelling after dissolving is the key step to create hierarchical porous architectures, while freezing medium plays a very important role in tailoring the hierarchical porous structure of aerogel and its carbon. This dissolving-gelling method is supposed to be a new strategy to create novel 3D hierarchical porous aerogels and carbon aerogels from chitosan for various applications.

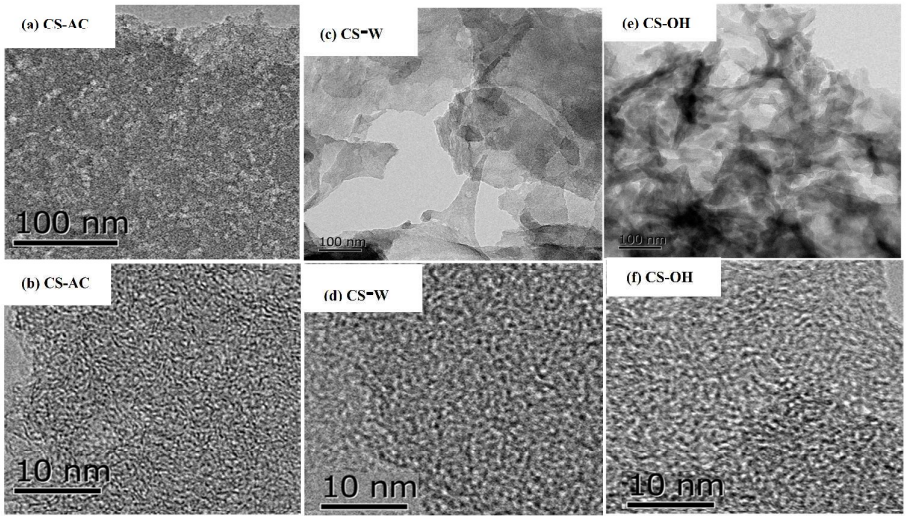

Figure 2. TEM images of CS-AC (a and b), CS-W (c and d), and CS-OH (e and f).

TEM images show that CS-AC has a sheet-like microstructure (Figure 2a), and the sheets are less transparent under electron beam irradiation. This indicates that the sheets are quite large and thick, which is consist with the result from SEM. For CS-W (Figure 2c), the sheets are much smaller and more transparent, indicating that the new preparation process produced thinner sheets with much smaller diameter. In the case of CS-OH, however, large amounts of nanorods can be clearly observed (Figure 2e), which again conforms the nanorod interconnected structure. High-resolution TEM images (Figure 2b, 2d, and 2f) further demonstrate the porous structure

with numerous micropores (less than 3 nm). These well-developed micropores are expected to provide an efficient path for the transportation and penetration of ions, favoring the fast transfer of ions[43]. Furthermore, lattice fringes (aligned graphitic layers) can be observed in Figure 2b, 2d, and 2f, which correspond to the graphite (002) plane, implying partial graphitic structures. The results reveal that these porous carbons are composed of large amount of amorphous carbon and small quantity of graphitic structure. TEM, combined with SEM, demonstrates that CS-W and CS-OH have a well-developed hierarchical porous structure.

The microstructures of these porous carbons were further characterized by XRD and Raman spectra, and the results are displayed in Figure 3a and 3b, respectively. The intensive and weak diffraction peaks located at 2ϑ=24.4° and 43° (Figure 3a) are corresponding to the (002) and (100) planes, respectively[38]. The broad width of the reflections implies that the samples have more amorphous regions. Figure 3b shows that all samples have a broad D band at about 1335 cm^{-1} and a G band at about 1585 cm^{-1}, which are associated with the defect sites or disordered sp^2-hybridized carbon atoms of graphite and the graphite in-plane vibrations of sp^2-bonded carbon atoms, respectively[44,45]. The intensity of the D band is obviously higher than that of the G band for all samples, indicating a higher amorphous carbon concentration in the porous carbons. These results well agree with those from TEM and XRD.

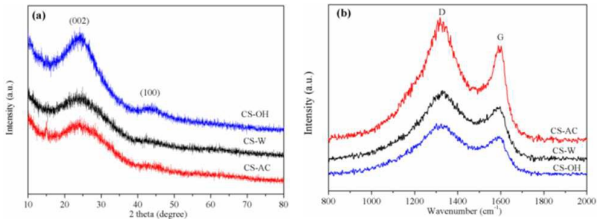

Figure 3. The XRD profiles (a) and Raman spectra (b) of CS-AC, CS-W, and CS-OH.

Table 1. The contents of the main elements in the samples

Samples	C%	N%	H%
CS-W	71.1	5.47	1.14
CS-AC	70.49	4.73	1.62
CS-OH	76.06	5.71	1.17

The C, H, and N contents of the samples were detected by elemental analysis, and the results are listed in Table 1. CS-W and CS-OH show higher N contents (5.47% and 5.71%, respectively), while CS-AC has a less N content (4.73%), showing that more N (more than 5%) can be doped in the skeleton of the hierarchical carbons by using this dissolving-gelling method. To understand the nature of N species, XPS was employed to evaluate the chemical nature of the carbon element and the presence and type of N in these carbon networks, as shown in Figure 4. There are three peaks, e.g. C1s, N1s, and O1s exist in all samples (Figure 4a). The high resolution N1s spectra are deconvolved (Figure 4b-d). For all samples, the deconvolutions of the N1s spectra can be fitted by four component peaks, which are ascribed to pyridinic N (N-6, 398.4 eV), pyrrolic/pyridone N (N-5, 400.7 eV), quaternary N (N-Q, 401.2 eV), and pyridine-N-oxide (N-X, 403.8 eV)[34,46].

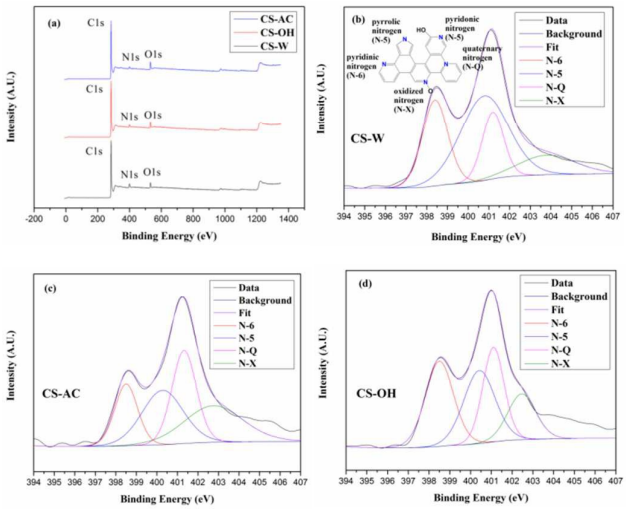

Figure 4. XPS spectra of CS-AC, CS-W, and CS-OH: (a) survey, (b) N1s of CS-W, (c) N1s of CS-AC, (d) N1s of CS-OH.

N atoms located at the edge of graphene layers, e.g. N-6 and N-5, are considered to represent the pseudo-capacitance effect, while the N functionalities located at the middle of graphite (N-Q) are generally less active than other N functionalities[46,47]. Table 2 summarizes the relative integral contents of various N atoms in the N1s spectra. It shows that the ratios of N-6/N and N-5/N are 25.00% and 46.30% for CS-W, 29.76% and 28.57 for CS-OH, 17.52% and 27.68% for CS-AC, respectively. These results, in combining with the total doped N contents (Table 1), indicate that CS-W and CS-AC have the highest and the lowest edge-N, respectively, which may have influence on the electrochemical performances of these N-self-doped carbons[28,47]. However, how the hierarchical porous structure of aerogel precursor influences the doped N type and content in carbon network is still unknown.

Table 2. The contents of different types of N

Samples	N-6 (%)	N-5 (%)	N-Q (%)	N-X (%)
CS-W	25.00	46.30	16.20	12.50
CS-OH	29.76	28.57	25.60	16.07
CS-AC	17.52	27.68	28.25	26.55

The N_2 adsorption/desorption isotherm and pore-size-distribution (PSD) curves of these porous carbons are depicted in Figure 5. According to the classification of IUPAC, all samples display IV adsorption isotherm. A short hysteresis loop at a higher relative pressure indicates numerous mesopores and macropores existed in these porous carbons. A more significant hysteresis for CS-OH indicates much more mesopores in this porous carbon[48]. A sharp increase at low relative pressure implies the existence of micropores[49,50]. Figure 5b again confirms that CS-OH has much more micropores (less than 2 nm) and mesopores (2-50 nm) than CS-W and CS-AC, while CS-AC has the least micropores and

mesopores. These results well agree with SEM analysis. Table 3 shows that the micropore volume and micropore specific area are 0.227cm^3/g and 432 m^2/g for CS-AC, 0.247 cm^3/g and 470 m^2/g for CS-W, 0.454 cm^3/g and 863 m^2/g for CS-OH, indicating that CS-OH has much more micropores. For this reason, CS-OH exhibits a much higher BET value (1408 m^2/g) than CS-W (554 m^2/g) and CS-AC (496 m^2/g).

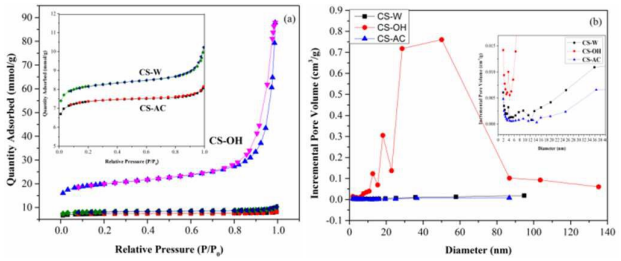

Figure 5. Nitrogen adsorption/desorption isotherms (a) and pore size distributions (b) of hierarchical porous carbons.

Table 3. Textural properties and CO_2 uptakes of porous carbons.

Sample	CS-AC	CS-W	CS-OH
S_{BET} (m^2/g)	496	554	1408
S_{micro}(m^2/g)	432	470	863
$V_{Micropore}$ (cm^3/ g)	0.227	0.247	0.454
CO_2 uptake (mmol/g)	3.07	3.44	3.27

A BET value of higher than 1400 m^2/g is comparable to those of other chitosan-derived porous carbons, such as silica-templated porous carbon (about 1000 m^2/g)[37,51], silica-templated and nickel nitrate-catalyzed porous carbon (977 m^2/g)[38], and even B, N-codoped porous carbon (710 m^2/g)[52]. These results, combined with SEM and TEM, show typical 3D hierarchical porous carbons. The micropores and partial mesopores originated from pyrolysis at high temperature, while maropores and the rest mesopores were developed in the gelling process. Therefore, we can easily tailor the hierarchical porous structure of the N-self-doped carbon by controlling the dissolving-gelling and freeze-drying conditions. More importantly, we can obtain porous carbon with high specific surface area and various pores without any activator, catalyst, and/or porogen.

CO_2 capture is gaining increasing attention due to its critical role in global climate change. Since carbon-based materials have a variety of advantages, such as low cost, large pore volume, hydrophobicity, high thermal stability, and low energy consumption for regeneration, etc.[53,54]. Therefore, CO_2 capture by porous carbons has spurred great interest[55-58]. Because our hierarchical porous N-self-doped carbons have high surface area and large amounts of pores as well as doped N functionalities, we investigated the possibility of using these carbons in CO_2 capture, and the results are shown in Table 3 and Figure 6. It can be clearly seen that CO_2 adsorption capacity increases with CO_2 pressure for all samples; and the CO_2 uptakes are 3.07 mmol/g for CS-AC, 3.44 mmol/g for CS-W, and 3.27 mmol/g for CS-OH. CS-AC shows the lowest CO_2 uptake, which can be attributed to the least micropores and mesopores. CS-OH with the most micropores and mesopores, however, does not show the highest CO_2 uptake, which may be due to a large number of scattered micropores that are too small to absorb and accommodate CO_2 molecule. These results show that CO_2 uptake capacity is not directly proportional to the specific surface area of material, and similar phenomenon was also reported in previous work[58]. Therefore, a precise control of the porosity of carbon is required to fabricate high-performance CO_2 sorbents.

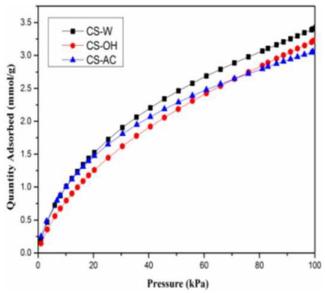

Figure 6. CO_2 adsorption curves of N-self-doped carbons at 298 K.

The CO_2 uptake capacities of CS-W and CS-OH are higher than those of carbons with and without N doping, such as carbon nitride spheres based on cellular silica foams (2.90 mmol/g)[59], activated charcoals and biochars (1.0-2.5 mmol/g)[60], activated carbon derived from coffee grounds (2.6 mmol/g)[61], which can be ascribed to the unique porous structure with reasonable porosity and hierarchical pores including micropores, mesopores, and macropores. We also believe that the CO_2 uptake capacity of CS-OH will be significantly improved by further tailoring its porous structure.

Electrochemical performances

Figure 7 shows the cyclic voltammetry and charge-discharge curves as well as specific capacitances of N-self-doped carbons. Figure 7a shows that all cyclic voltammetry curves display quasi-rectangular shapes, and the cyclic voltammetry curve of CS-W has a larger area than those of CS-AC and CS-OH, suggesting that CS-W has a higher specific capacitance. The charge-discharge curves of these samples at 1.0 A/g (Figure 7b) are not strictly symmetrical and are slightly distorted, implying the pseudo-capacitive behavior of active functional groups[45,62,63]. The specific capacitances of CS-AC, CS-W, and CS-OH are 181, 241, and 167 F/g at a current density of 1.0 A/g, respectively. It is unpredictable that CS-OH, which has the highest BET value, shows the lowest specific capacitance, indicating that the specific capacitance is not proportional to the specific surface area. Obviously, some micropores in CS-OH are not accessible to electrolytes. CS-W has a higher specific capacitance than CS-AC, which can be ascribed to the unique hierarchical porous structure with reasonable macropores, mesopores and micropores, as shown in Figure 1, Figure 2, Figure 5, and Table 3. The thinner and porous walls of CS-W may also facilitate the diffusion and storage of ions.

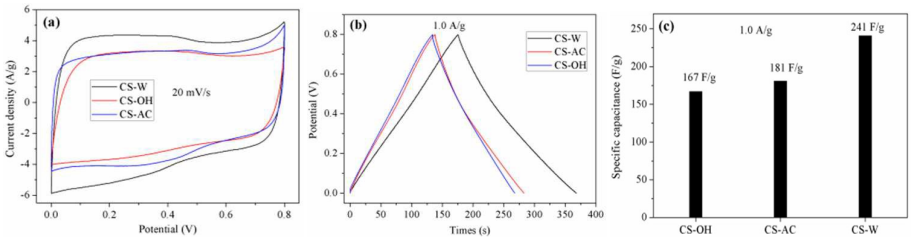

Figure 7. Cyclic voltammetry curves at the a scanning rate of 20 mV/s in 1.0 M H_2SO_4 (a), charge-discharge curves at a current density of 1.0 A/g (b), and the specific capacitances (1.0 A/g) of N-self-doped porous carbons (c).

To further demonstrate the electrochemical properties of CS-W for supercapacitor, its cyclic voltammetry performance at different scanning rates and charge-discharge property at different current densities were investigated, as shown in Figure 8. The CV curves are still quasi-rectangular without clear distortion at high scanning rate (Figure 8a), and the specific capacitance of CS-W from CV testing decreases from 474 to 328 F/g (Figure 8b) as the scanning rate increases from 2 mV/s to 100 mV/s, indicating a high conductivity to assure excellent charge propagation.

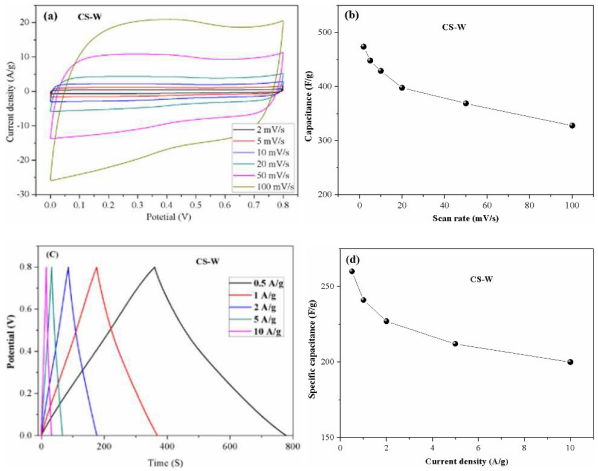

Figure 8. The cyclic voltammetry curves (a) and specific capacitances from cyclic voltammetry testing (b) at different scanning rates; charge-discharge curves (c) and specific capacitances from charge-discharge testing (d) at different current densities.

Figure 8c and 8d demonstrate the charge-discharge curves and specific capacitances of CS-W at different current densities. The specific capacitance of CS-W is 261 F/g at 0.5 A/g, and remains 200 F/g even at a current density of 10 A/g, suggesting a very attractive rate capability. The voltage drop at the initiation of the discharge is extremely small even at a high current density of 10 A/g, indicating a very low equivalent series resistance (ESR)[42]. The cycling performance of CS-W displays a negligible capacitance degradation after 5000 cycles (Figure S1). The capacitance retains 96% of the initial specific capacitance in 1.0 M H_2SO_4, indicating that CS-W is a very stable electrode material.

Table 4 shows the comparison of various carbons in electrochemical capacitive performance. CS-W which was prepared by dissolving-gelling method without activator, nanoporogen, and catalyst in this work has a high specific capacitance (200-261 F/g at current densities of 0.5 -10 A/g) that is not only superior to that of chitosan-based carbon aerogel (about 291 F/g at 2 mV/s) obtained by directly freeze-drying in aqueous acetic acid and subsequently chemical activation[42], but also superior to those of other chitosan-derived carbons, such as silica-templated and nickel nitrate-catalyzed mesoporous carbon (222 F/g at 0.5 A/g)[38], and even B, N-codoped porous carbon (about 250 F/g at 0.5 A/g)[52]. Moreover, a specific capacitance of 261 F/g is higher than those of N-doped carbons derived from other biomass resources, such as human hair (about 150 F/g at 1.0 A /g)[64], KOH activated argan seed shell (about 230 F/g at 1.0 A/g)[65], pitch (294 F/g at 2 mV/s)[66], and those of nano carbon materials like graphene/CNT hybrid films (124 F/g at 10 mV/s)[67], N-doped graphene sheets (144.9 F/g at 0.5 A/g)[68]. The prominent capacitance performance of CS-W can be ascribed to the unique porous structure created by the dissolving-gelling process. The desirable hierarchical framework with well-developed micropores, mesopores, and macropores facilitates the transport of electrolytes and electrons with a lower resistance.

Table 4. Comparison of various carbons in electrochemical capacitive performance.

Carbons [a]	Condition [b]	Capacity (F/g)	Ref.
CS-derived C	0.1 M KOH	222, 0.5 A/g	38
CS-derived C	6 M KOH	291, 2 mV/s	42
B, N-codoped C	1 M H_2SO_4	250, 0.5 A/g	52
Hair-derived C	1 M KOH	150,1.0 A/g	64
ASS-derived C	1 M H_2SO_4	230, 1.0 A/g	65
Pitch-derived C	6 M KOH	294, 2 mV/s	66
Graphene/CNT	1 M H_2SO_4	124, 10 mV/s	67
N-doped graphene	Organic solvent	144.9,0.5 A/g	68
CS-W	1 M H_2SO_4	261, 0.5 A/g	This work
	1 M H_2SO_4	474, 2 mV/s	

[a] CS, C, and ASS refer to chitosan, carbon, and argan seed shell, respectively. [b] Three-electrode test system.

Figure 9 shows the electrochemical impedance spectroscopic (EIS) of CS-W, CS-AC, and CS-OH. In the low-frequency region, CS-W, CS-AC, and CS-OH have a steep capacitive spike with an almost 90° angle, indicating a good capacitive behavior (vertical line for an ideal capacitor). The real axis intercept corresponds to the equivalent series resistance (ESR), whereas the radius of the semicircle impedance of electrode materials commonly represents charge-transfer resistance between electrode material and the

electrolyte. Obviously, CS-W displays a semicircle impedance that is smaller than those of CS-AC and CS-OH at a high frequency region, revealing that CS-W has a lower charge-transfer resistance. However, CS-AC has a much larger semicircle impedance than CS-AC and CS-OH, indicating a high charge-transfer resistance. The ESR of CS-W (1.24 Ω) also is lower than those of CS-AC (1.46 Ω) and CS-OH (1.35 Ω). The less resistance of CS-W should be attributed to the hierarchical structure with desirable hierarchical pores (Figure 1b, Figure 5b, and Table 3) that can shorten the path of external electrolyte to the interior network. For CS-AC, thicker pore walls (Figure 1a and Figure 2a) with less micropores and especially mesopores (Figure 1a, Figure 5b, and Table 3) disfavor ion diffusion and result in a longer distance of ion diffusion, and thus the resistance is high.

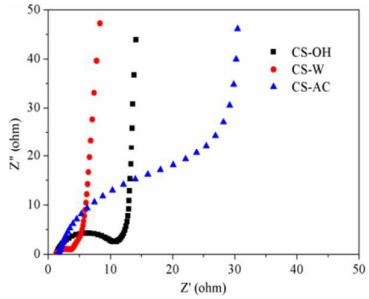

Figure 9. Nyquist plots of CS-AC, CS-W, and CS-OH.

Overall, the 3D hierarchical porous N-self-doped carbons obtained by dissolving-gelling method shows a prominent capacitance performance. The main advantages of our strategy over other synthetic methods reported previously for preparing chitosan-derived carbon materials are: (1) hierarchical porous structure with widely distributed pores as well as high specific surface area can be obtained by a unique dissolving-gelling method without any activator, nanoporogen, catalyst or post treatment; (2) the hierarchical porous structure can be easily tailored by controlling the gelling and subsequent freeze-drying condition. These advantages, in combination with the unique physicochemical features, excellent electrochemical and CO_2 capture performances, as well as the superior advantages of raw material such as renewability, abundance, low cost, environmentally friendly, make these sustainable N-self-doped carbons promising and high-performance porous carbon materials for supercapacitor and CO_2 capture. We can also foresee that these N-self-doped carbons will become ideal supports for metals and metal oxides for applications in electrochemical catalysis. Especially, CS-OH with unique nanorod interconnected structure and high specific surface area is supposed to be a promising hierarchical porous carbon that can be used in energy storage and catalysis by further controlling its microstructure.

Conclusions

We designed an effective strategy to produce hierarchical porous N-self-doped carbons and tailor their porous structures for supercapacitor and CO_2 capture applications. The most unique feature and advantage of this dissolving-gelling method is that chitosan could be dissolved in NaOH/urea/H_2O solution at low temperature and then easily gelled at room temperature. The gelling step created a 3D interconnected nanofibril network due to the aggregation of chitosan, and thus creating hierarchical porous N-self-doped carbons with well-developed macropores, mesopores, and micropore without any porogen, catalyst, and activator. Freezing medium plays a very important role in tailoring the hierarchical porous structure, and nanorod interconnected and fiber-wall interconnected architectures could be obtained by using tert-butanol and H_2O as a freezing medium, respectively. The nanorod interconnected N-self-doped carbon displayed a high specific surface area of 1408 m^2/g, while fiber-wall interconnected carbon exhibited a high specific capacitance of 261 F/g (0.5 A/g) due to the unique hierarchical porous structures. Furthermore, these hierarchical porous carbons had high CO_2 uptake capacities. This dissolving-gelling method is supposed to be a new and effective strategy to create novel sustainable 3D hierarchical porous aerogels and N-self-doped porous carbons from chitosan for various applications.

Acknowledgements

This work was supported by State Key Laboratory of Pulp and Paper Engineering (2015QN05), National Natural Science Foundation of China (21506068), Pearl River S&T Nova Program of Guangzhou, Guangdong natural Science Foundation (2014A030310319), Major State Basic Research Projects of China (973-2012CB215302), Fundamental Research Funds for the Central Universities.

Notes and references

1 X.L. Wu and A. W. Xu, *J. Mater. Chem. A*, 2014, **2**, 4852-4864.
2 Y. Zhai, Y. Dou, D. Zhao, P. F. Fulvio, R. T. Mayes and S. Dai, *Adv. Mater.*, 2011, **23**, 4828-4850.
3 G. Wang, L. Zhang and J. Zhang, *Chem. Soc. Rev.*, 2012, **41**, 797-828.
4 L. Hao, X. Li and L. Zhi, *Adv. Mater.*, 2013, **25**, 3899-3904.
5 K. Jost, C. R. Perez, J. K. McDonough, V. Presser, M. Heon, G. Dion and Y. Gogotsi, *Energ. Environ. Sci.*, 2011, **4**, 5060-5067.
6 L. Ji, Z. Lin, M. Alcoutlabi and X. Zhang, *Energ. Environ. Sci.*, 2011, **4**, 2682-2699.
7 S. Nardecchia, D. Carriazo, M. L. Ferrer, M. C. Gutiérrez and F. del Monte, *Chem. Soc. Rev.*, 2013, **42**, 794-830.
8 D. W. Wang, F. Li, M. Liu, G. Q. Lu and H.-M. Cheng, *AngewandteChemie*, 2008, **120**, 379-382.
9 K. Xia, Q. Gao, J. Jiang and J. Hu, *Carbon*, 2008, **46**, 1718-1726.
10 Y. Wu, G. Gao and G. Wu, *J. Mater. Chem. A*, 2015, **3**, 1828-1832.
11 R. Liu, L. Wan, S. Liu, L. Pan, D. Wu and D. Zhao, *Adv. Funct. Mater.*, 2015, **25**, 526-533.
12 Z. S. Wu, Y. Sun, Y.-Z. Tan, S. Yang, X. Feng and K. Müllen, *J. Am. Chem. Soc.*, 2012, **134**, 19532-19535.
13 D. Yu, K. Goh, H. Wang, L. Wei, W. Jiang, Q. Zhang, L. Dai and Y. Chen, *Nat. nanotechnol.*, 2014, **9**, 555-562.
14 S. He, H. Hou and W. Chen, *J. Power Sources*, 2015, **280**, 678-686.
15 W. Gu and G. Yushin, Wiley Interdisciplinary Reviews: Energy and Environment, 2014, **3**, 424-473.

16 K. N. Wood, R. O'Hayre and S. Pylypenko, *Energ. Environ. Sci.*, 2014, **7**, 1212-1249.
17 K. Mamtani and U. S. Ozkan, *Catal. Lett.*, 2015, **145**, 436-450.
18 J. P. Paraknowitsch and A. Thomas, *Energ. Environ. Sci.*, 2013, **6**, 2839-2855.
19 S. Gao, H. Fan, Y. Chen, L. Li, Y. Bando and D. Golberg, *Nano Energy*, 2013, **2**, 1261-1270.
20 Y. Lu, F. Zhang, T. Zhang, K. Leng, L. Zhang, X. Yang, Y. Ma, Y. Huang, M. Zhang and Y. Chen, *Carbon*, 2013, **63**, 508-516.
21 K. Jurewicz, R. Pietrzak, P. Nowicki and H. Wachowska, *Electrochim. Acta*, 2008, **53**, 5469-5475.
22 L. L. Zhang and X. Zhao, *Chem. Soc. Rev.*, 2009, **38**, 2520-2531.
23 W. Luo, B. Wang, C. G. Heron, M. J. Allen, J. Morre, C. S. Maier, W. F. Stickle and X. Ji, *Nano Lett.*, 2014, **14**, 2225-2229.
24 X. Yang, J. Li, J. Liu, Y. Tian, B. Li, K. Cao, S. Liu, M. Hou, S. Li and L. Ma, *J. Mater. Chem. A*, 2014, **2**, 1550-1559.
25 M. Yang, Y. Zhong, L. Su, J. Wei and Z. Zhou, *Chem.-Eur. J.*, 2014, **20**, 5046-5053.
26 E. Fiset, T. E. Rufford, M. Seredych, T. J. Bandosz and D. Hulicova-Jurcakova, *Carbon*, 2015, **81**, 239-250.
27 S. Zhang, K. Dokko and M. Watanabe, *Chem. Mater.*, 2014, **26**, 2915-2926.
28 X. Ning, W. Zhong, S. Li, Y. Wang and W. Yang, *J. Mater. Chem. A*, 2014, **2**, 8859-8867.
29 K. T. Cho, S. B. Lee and J. W. Lee, *J. Phys. Chem. C*, 2014, **118**, 9357-9367.
30 H. Ren, H. Tian, H.-S. Lee, T. Park, F. C. Leung, T.-L. Ren and J. Chae, *Nano Energy*, 2015, **15**, 697-708.
31 H. Zhu, J. Yin, X. Wang, H. Wang and X. Yang, *Adv. Funct. Mater.*, 2013, **23**, 1305-1312.
32 Y. S. Yun, S. Y. Cho and H. J. Jin, *Macromol. Res.*, 2014, **22**, 509-514.
33 Y. S. Yun, S. Y. Cho, J. Shim, B. H. Kim, S. J. Chang, S. J. Baek, Y. S. Huh, Y. Tak, Y. W. Park and S. Park, *Adv. Mater.*, 2013, **25**, 1993-1998.
34 Z. Li, Z. Xu, X. Tan, H. Wang, C. M. Holt, T. Stephenson, B. C. Olsen and D. Mitlin, *Energ. Environ. Sci.*, 2013, **6**, 871-878.
35 X. Y. Chen, C. Chen, Z. J. Zhang and D. H. Xie, *J. Mater. Chem. A*, 2013, **1**, 10903-10911.
36 Y. Liang, H. Liu, Z. Li, R. Fu and D. Wu, *J. Mater. Chem. A*, 2013, **1**, 15207-15211.
37 T -D. Nguyen, K. E. Shopsowitz and M. J. MacLachlan, *J. Mater. Chem. A*, 2014, **2**, 5915-5921.
38 Q. Liang, H. Su, J. Yan, C. Leung, S. Cao and D. Yuan, *Chinese. J. Catal.*, 2014, **35**, 1078-1083.
39 M. Leżańska, A. Olejniczak, A. Pacuła, G. Szymański and J. Włoch, *Catal. Today*, 2014, **227**, 223-232.
40 P. Hao, Z. Zhao, J. Tian, H. Li, Y. Sang, G. Yu, H. Cai, H. Liu, C. Wong and A. Umar, *Nanoscale*, 2014, **6**, 12120-12129.
41 M. Zhi, C. Xiang, J. Li, M. Li and N. Wu, *Nanoscale*, 2013, **5**, 72-88.
42 P. Hao, Z. Zhao, Y. Leng, J. Tian, Y. Sang, R. I. Boughton, C. Wong, H. Liu and B. Yang, *Nano Energy*, 2015, **15**, 9-23.
43 J. Hou, C. Cao, X. Ma, F. Idrees, B. Xu, X. Hao and W. Lin, *Sci. rep-uk*, 2014, **4**.
44 J. Ding, H. Wang, Z. Li, A. Kohandehghan, K. Cui, Z. Xu, B. Zahiri, X. Tan, E. M. Lotfabad and B. C. Olsen, *ACS nano*, 2013, **7**, 11004-11015.
45 L. Sun, Y. Fu, C. Tian, Y. Yang, L. Wang, J. Yin, J. Ma, R. Wang and H. Fu, *ChemSusChem*, 2014, **7**, 1637-1646.
46 B. Xu, S. Hou, G. Cao, F. Wu and Y. Yang, *J. Mater. Chem.*, 2012, **22**, 19088-19093.
47 C. O. Ania, V. Khomenko, E. Raymundo-Piñero, J. B. Parra and F. Beguin, *Adv. Funct. Mater.*, 2007, **17**.
48 H. Wang, D. Zhang, T. Yan, X. Wen, J. Zhang, L. Shi and Q. Zhong, *J. Mater. Chem. A*, 2013, **1**, 11778-11789.
49 C. H. Huang, Q. Zhang, T. C. Chou, C. M. Chen, D. S. Su and R. A. Doong, *ChemSusChem*, 2012, **5**, 563-571.
50 B. Chang, Y. Guo, Y. Li, H. Yin, S. Zhang, B. Yang and X. Dong, *J. Mater. Chem. A*, 2015, **3**, 9565-9577.
51 A. Olejniczak, M. Lezanska, J. Wloch, A. Kucinska and J. P. Lukaszewicz, *J. Mater. Chem. A*, 2013, **1**, 8961-8967.
52 Z. Ling, G. Wang, M. Zhang, X. Fan, C. Yu, J. Yang, N. Xiao and J. Qiu, *Nanoscale*, 2015, **7**, 5120-5125.
53 A. Stein, Z. Wang and M. A. Fierke, *Adv. Mater.*, 2009, **21**, 265-293.
54 G. P. Hao, W. C. Li and A. H. Lu, *J. Mater. Chem.*, 2011, **21**, 6447-6451.
55 Y. Zhang, B. Li, K. Williams, W.-Y. Gao and S. Ma, *Chem. Commun.*, 2013, **49**, 10269-10271.
56 X. Fan, L. Zhang, G. Zhang, Z. Shu and J. Shi, *Carbon*, 2013, **61**, 423-430.
57 R. Wang, P. Wang, X. Yan, J. Lang, C. Peng and Q. Xue, *Acs Appl. Mater. Interfaces*, 2012, **4**, 5800-5806.
58 M. Sevilla and A. B. Fuertes, *Energ. Environ. Sci.*, 2011, **4**, 1765-1771.
59 Q. Li, J. Yang, D. Feng, Z. Wu, Q. Wu, S. S. Park, C. S. Ha and D. Zhao, *Nano. Res.*, 2010, **3**, 632-642.
60 Y. F. Huang, P. T. Chiueh, C. H. Shih, S. L. Lo, L. Sun, Y. Zhong and C. Qiu, *Energy*, 2015, **84**, 75-82.
61 M. Plaza, A. González, C. Pevida, J. Pis and F. Rubiera, *Appl. Energ.*, 2012, **99**, 272-279.
62 L. F. Chen, X.-D. Zhang, H. W. Liang, M. Kong, Q. F. Guan, P. Chen, Z. Y. Wu and S. H. Yu, *ACS nano*, 2012, **6**, 7092-7102.
63 Y. Xu, Z. Lin, X. Huang, Y. Wang, Y. Huang and X. Duan, *Adv. Mater.*, 2013, **25**, 5779-5784.
64 Z. Guo, Q. Zhou, Z. Wu, Z. Zhang, W. Zhang, Y. Zhang, L. Li, Z. Cao, H. Wang and Y. Gao, *Electrochim. Acta*, 2013, **113**, 620-627.
65 A. Elmouwahidi, Z. Zapata-Benabithe, F. Carrasco-Marín and C. Moreno-Castilla, *Bioresource Technol.*, 2012, **111**, 185-190.
66 Q. Wang, J. Yan, Y. Wang, T. Wei, M. Zhang, X. Jing and Z. Fan, *Carbon*, 2014, **67**, 119-127.
67 D. Yu and L. Dai, *J. Phys. Chem. Lett.*, 2009, **1**, 467-470.
68 Y. Qiu, X. Zhang and S. Yang, *Phys. Chem. Chem. Phys.*, 2011, **13**, 12554-12558.

Graphical Abstract